NANO LETTERS

pubs.acs.org/NanoLett

Letter

Cylindrical Line-Feeding Growth of Free-Standing Silicon Nanohelices as Elastic Springs and Resonators

Haiguang Ma, Rongrong Yuan, Junzhuan Wang, Yi Shi, Jun Xu, Kunji Chen, and Linwei Yu*

Cite This: *Nano Lett.* 2020, 20, 5072−5080

Read Online

ACCESS | Metrics & More | Article Recommendations | Supporting Information

ABSTRACT: Three-dimensional (3D) construction of free-standing silicon (Si) nanohelices has been a formidable challenge for planar lithography and etching technology. We here demonstrate a convenient 3D growth and integration of Si nanohelices (SiNHs) upon bamboolike cylinders with corrugated sidewall grooves, where the indium catalyst droplets grow around the cylinders in a helical fashion, while consuming precoated amorphous Si (a-Si) thin film to produce crystalline Si nanowires on the sidewalls. At the end of each groove cycle, the droplets are enforced to linefeed/switch into the neighbor groove to continue a spiral growth of SiNHs with readily tunable diameter, pitch, aspect-ratio, and chiral/achiral symmetries. In addition, the SiNHs can be reliably released as free-standing units to serve as elastic links, supports and vibrational resonators. These results highlight the unexplored potential of high precision 3D self-assembly growth in constructing a wide range of sophisticated electromechanical, sensor, and optoelectronic functionalities.

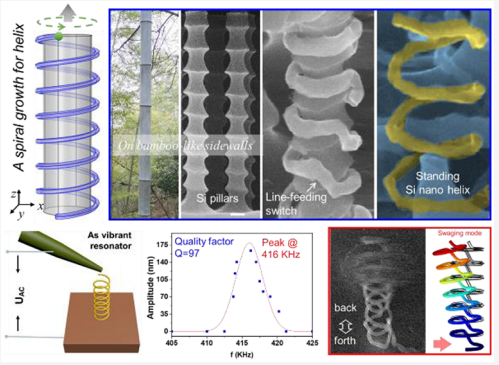

KEYWORDS: *Silicon nanowires, free-standing nanohelices, 3D self-assembly growth*

In the past decade, precise patterning and fabrication of three-dimensional (3D) nanostructures, such as stacked or vertical channels,[1−7] cantilevers,[8−10] bioprobes,[11,12] or helical complexes,[13−18] have attracted intensive research efforts, as they hold great potential for developing a new generation of nanoelectromechanical system (NEMS),[8−10,19] electronics,[1−7] and sensor[8,11,12] applications. However, conventional planar lithography technology is difficult or inefficient to construct these 3D nanostructures. Recently, many sophisticated approaches have been developed, including glancing angle or focused beam-assisted depositions,[20−22] two-photon 3D lithography,[23−25] or origami folding,[26−28] in order to fabricate various nanoscale 3D complexes. Among them, nanohelix (NH) represents a fundamental type of building block that has been widely used for achieving enhanced elasticity,[13] chirality,[14,15] and sensitivity in optical or NEMS applications.[16−18]

Though 3D nanowire (NW) coils,[29−33] double helices,[34,35] and carbon nanotubes coils[36,37] have been synthesized via low cost and high yield self-assembly approaches, there are still formidable difficulties to integrate them for scalable electronic devices. So, seeking a high precision self-assembly growth, combining the strength of top-down lithography and the diversity of bottom-up approach, will help to greatly extend the capabilities of conventional planar processing to fabricate more complex and advanced 3D nanostructures. Actually, producing a standing helix, as depicted in Figure 1a, requires only a spiral growth of 1D NW on the curved sidewall surface of a cylinder. However, this sidewall growth confinement is hard to impose for the vapor−liquid−solid (VLS) growth of NWs, as the gaseous precursor feeding usually encourages out-of-plane instead of in-plane growth of NWs.[38−40] This challenge could be better addressed by resorting to a relatively new in-plane solid−liquid−solid (IPSLS) growth mechanism, established in our previous works,[41−44] which can help to confine the growth of SiNWs on substrate surface that is covered by amorphous Si (a-Si) layer as a precursor. However, the potential of this technology in constructing more complex and functional 3D SiNHs has hitherto not been explored.

Inspired by the spiral growth of slim vines around trees (Figure 1b), we here demonstrate a novel spiral line-feeding growth of self-standing Si NHs upon the sidewalls of bamboolike cylinders. The sidewall grooves are formed by simple Bosch-etching into Si wafer, providing critical guidance for the indium (In) catalyst droplets to circle around the cylinder in a compact helical fashion with line-feeding switching at the end of each cycle. The resulting SiNHs can be batch-fabricated and safely released as self-standing units with designable geometry and aspect-ratio laying a solid basis for exploring more advanced SiNH-based functionalities.

Received: March 23, 2020
Revised: June 9, 2020
Published: June 10, 2020

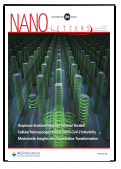

https://dx.doi.org/10.1021/acs.nanolett.0c01265
Nano Lett. 2020, 20, 5072−5080

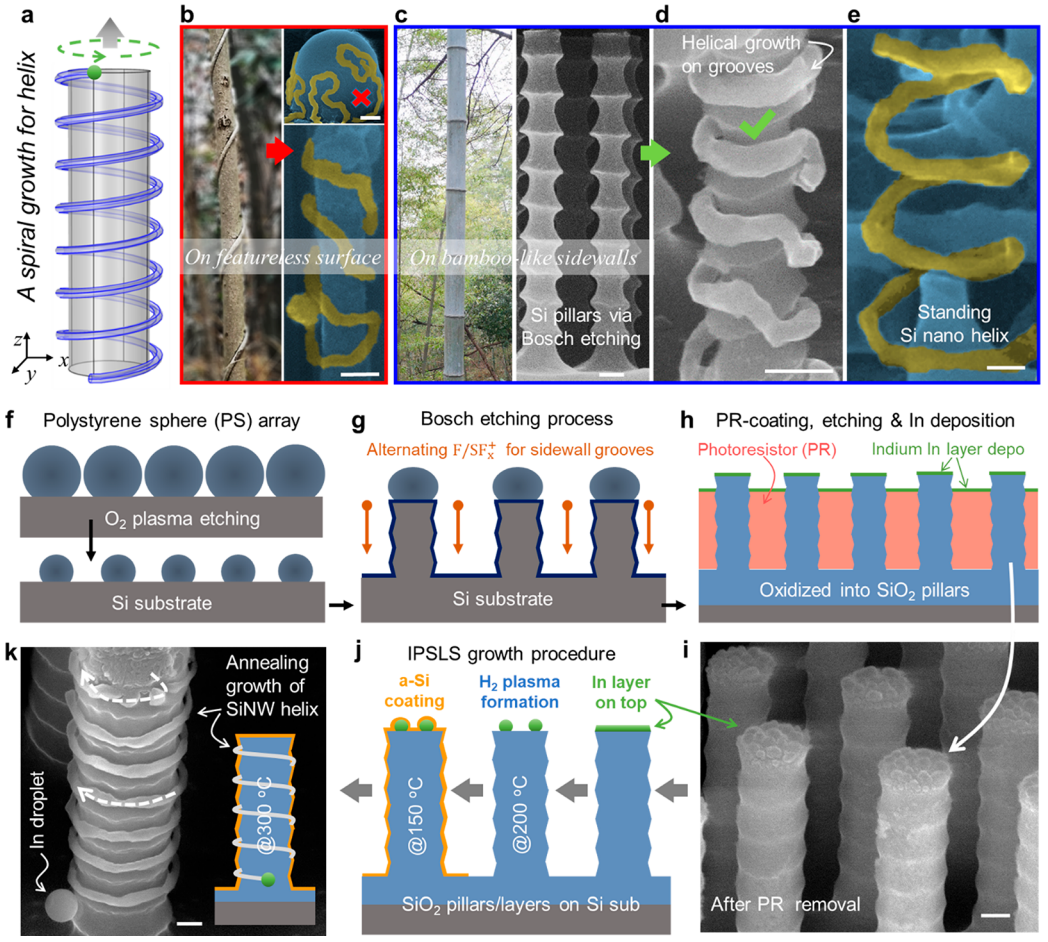

Figure 1. Spiral growth of nanowires on bamboolike cylinders. (a) Schematic illustration of a winding 3D growth of Si nanowires (SiNWs) on cylinder sidewall to form a helical structure. (b–e) Photographs or SEM images of the growth of quasi-1D plant or SiNWs on featureless and bamboolike corrugated sidewall surfaces, respectively. Scale bars in the top and bottom panels in (b) stand for 500 and 100 nm, while in (c–e) scale bars stand for 200, 200, and 100 nm, respectively. (f–h) Patterning, Bosch etching, and oxidation of Si wafer into standing pillars with periodic sidewall grooves using polystyrene sphere (PS) array as a template, followed by the filling of photoresistor (PR) layer, etching to expose the pillar tips, and deposition of indium (In) catalyst layer on top. (k) Oxidized pillars with In layer on top after removing the PR layer which are then processed via standard IPSLS growth procedure with H_2 plasma treatment for droplet formation and a-Si coating as depicted in (j). Finally, the sample was annealed at a relatively higher temperature to grow SiNWs that cycle down the cylinder to form continuous helical structure, as observed in (i) and illustrated in its inset. Scale bars in (i,k) are 200 nm.

As the SiNWs grown upon the featureless/smooth sidewalls are usually irregular, as seen for example in the scanning electron microscope (SEM) images shown in the right panels in Figure 1b, bamboolike columns with periodic sidewall grooves/loops are designed and fabricated, as seen in Figure 1c, to direct the SiNWs to travel around the full perimeter of a groove before switching to the neighbor vacant groove via a line-feeding (LF) transition (Figure 1d). Specifically, the columns were fabricated by taking a monolayer of polystyrene (PS) spheres as templates with initial diameters of 500 nm to 2 μm, which were shrunk by O_2 plasma burning to ~200 nm (Figure 1f). After that, corrugated columns of L_{col} = 1–2 μm high were formed by Bosch etching into the Si wafer with alternating SF_6 (etching) and C_4F_8 (passivation) periods. More SEM images of the PS templates and the corrugated columns are provided in Supporting Information (SI) Figure S1. Note that both the periodicity and depth of the sidewall grooves can be adjusted during the Bosch etching.[7] Here, the depth T_d and the pitch W_p of the sidewall grooves are controlled to form a parabolic shape with a cross-section profile of $T_d \sim W_p/2$. Then, the corrugated columns were completely or partially converted into SiO_2 via a wet or dry oxidation process. In the next step, the oxide columns were covered by a thick layer of photoresistor (PR), followed by etching to expose the tips, and depositing an In capping layer of 15–40 nm thick (see Figure 1h,i and SEM image in Figure S1c). After the removal of PR, the sample was loaded into a plasma-enhanced chemical vapor deposition (PECVD) system and treated by H_2 plasma at 200 °C to transform the In capping layer into discrete droplets, followed by the coating of 30–50 nm a-Si layer at 150 °C by pure SiH_4 plasma. Upon annealing at 300 °C, the In droplets were activated to absorb the a-Si layer and produce SiNWs, spiraling down the column (Figure 1k). At the end, the remnant a-Si layer can be preserved or selectively etched off by using low-temperature H_2 plasma etching at 150 °C. More experimental details are provided in the Experimental Section or in the previous works.[41–44]

In order to achieve a stable spiral growth of SiNWs upon the corrugated sidewalls, the sizes of the guiding grooves and the leading catalyst droplets have to be matched. Figure 2a–c showcases three typical size-matching situations as well as the

https://dx.doi.org/10.1021/acs.nanolett.0c01265
Nano Lett. 2020, 20, 5072–5080

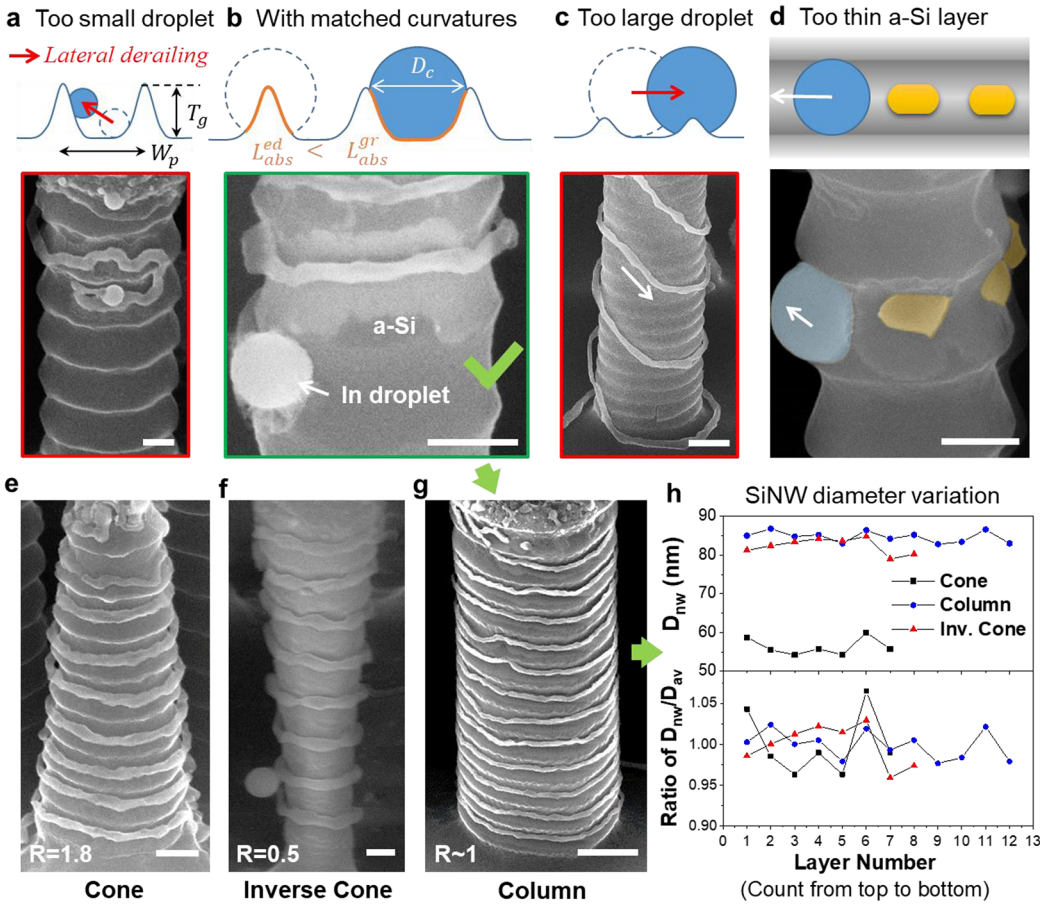

Figure 2. Stability and geometry control of helical growth. (a–c) Cross-section schematics and SEM images of the guided growths of SiNWs on the corrugated cylinder sidewalls under three distinct size-matching conditions, where the catalyst droplets are too small, matched, and too large compared to the sidewall grooves, respectively. The scale bars in (a–c) stand for 200 nm, 200 nm, and 1 μm. (d) The discontinuous sidewall growth caused by insufficient a-Si supply. (e–g) Stable helical growth accomplished upon cylinder sidewalls with conic ($R \equiv D_{col}^{root}/D_{col}^{top} > 1$), uniform ($R \sim 1$,) and inverse conic ($R < 1$) geometries, while the diameter variations of these SiNWs at different groove layers, counted from top to bottom, are extracted and plotted in (h). Scale bars in panels e–g are for 200 nm, 1 μm, and 200 nm, respectively.

SEM images of the resulted SiNWs in the lower panels. The following have been determined:

(1) For the sidewall growth led by too small catalyst droplets (Figure 2a), that is, the catalyst droplet diameter being much smaller than the groove dimensions, $D_c < 0.5W_p \sim T_d$, the droplet movement cannot be confined within the sidewall loops. Instead, as seen in the SEM image of Figure 2a, the small droplets can travel now freely on the wider slopes of the grooves and even steer back within the same track, undermining the basis for a spiral growth of SiNHs.

(2) On the contrary, for the case of SiNW growth led by relatively too large catalyst droplets (Figure 2c), the shallow grooves are insufficient to accommodate the In droplets, thus leaving the droplet to travel over the corrugations to produce random and loosely spaced SiNHs. This is usually observed when $D_c < 0.5W_p \sim T_d$ and also unfavorable for the growth of orderly and compact SiNHs.

(3) In between these two mismatched situations, as indicated by the red arrows in Figure 2a,c, there lies still a suitable parameter window for achieving a faithful sidewall guided growth of the SiNWs (Figure 2b), thus leading to well-defined SiNH structures.

In order to explain the observed stability phenomena, a simple heuristic local-curvature-matching judgment is proposed, which is based on the fact that the In droplets are driven by two competing trends, that is, (i) to stretch out to reach/absorb as much as possible the a-Si layer on the surface, which is the fundamental driving force for the in-plane growth, and (ii) to keep roughly a spherical shape to minimize the exposed surface/interface energy of the liquid catalyst droplet. Geometrically speaking, these two requirements can be better met if the local curvatures of the droplet ($\sim 2/D_c$) and the curved groove surface coated with a-Si can fit to each other, as depicted in Figure. 2b, that is, having similar absolute values but opposite signs (convex defined as positive). The contact with matched-curvature is favorable as it allows for the formation of the widest In/a-Si absorption front length of L_{abs}^{gr}, while keeping still a spherical shape, compared to the unfavorable situation residing over the edge tips (with positive and much larger curvature, in Figure. 2b), where the absorption front length over the edge is much less $L_{abs}^{ed} < L_{abs}^{gr}$. While a more comprehensive model has to take into account the influences of other growth balance conditions as detailed in our previous works,[42−46] this qualitative curvature-matching criterion is sufficient to explain most experimental observations and advise those seeking optimal structural designs. Note that at the end of each cycle the exhaustion of a-Si supply in the same groove will still force the droplet to climb over the groove edges to switch into the neighbor groove with a-Si coating, as described in more detail later.

https://dx.doi.org/10.1021/acs.nanolett.0c01265
Nano Lett. 2020, 20, 5072−5080

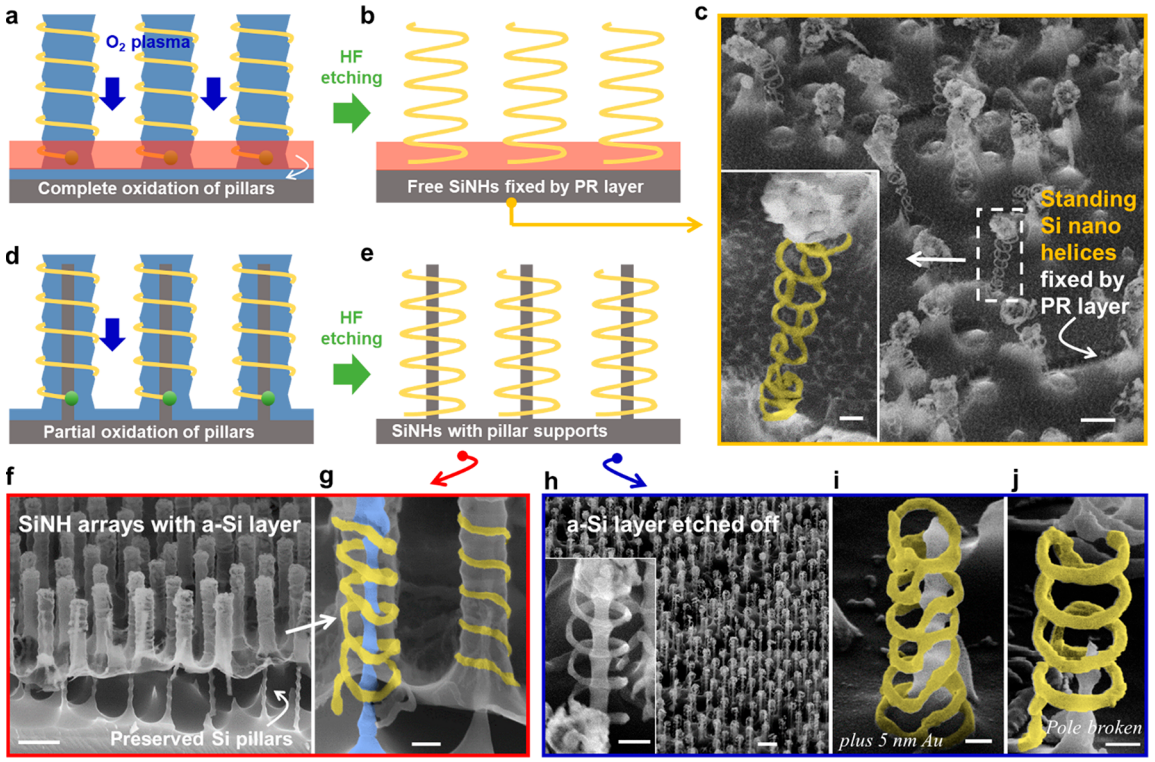

Figure 3. Standing helices by releasing SiNH array. (a,b) The releasing of continuous standing SiNWs grown on completely oxidized pillar sidewalls, by using bottom photoresistor (PR) layer fixation and subsequent hydrofluoric (HF) solution etching. The released SiNHs are shown in the SEM image in (c) with a bottom-left inset providing a close scrutiny. Scale bars in (c) and its inset stand for 1 μm and 200 nm, respectively. (d,e) The releasing of SiNHs from partially oxidized pillars via the same procedure. (f,g and h,i) The helices array with inner pillar supports with and without remnant a-Si layer, respectively. (i,j) Enlarged SEM images of standing SiNHs, coated with 5 nm gold to enhance SEM contrast with or without the thin pole at the center, respectively. Scale bars in (f,g) are 1 μm and 200 nm, while in (h), the inset of (h), (i), and (j) are 1 μm, 200 nm, 200 nm, and 200 nm.

The thickness of the a-Si precursor layer, coated on the sidewall grooves, is another critical parameter of control in seeking a uniform and continuous spiral growth of SiNHs. Similar to what happened for the planar IPSLS growth,[41,43,47] a shortage of a-Si supply, when the a-Si layer on the sidewall is too thin, will lead to a discrete growth (see Figure 2d) where despite roughly matched local curvatures/sizes the In droplet produces discrete islands decorated along the passed groove. In this work, the a-Si layer thickness has been first optimized, taking into account the slower deposition rate (typically 30% of that on planar surface) on the 3D sidewalls, to guarantee a continuous growth of SiNWs and even intentionally (~10%) thicker to counter the supply variation during LF-switching across the groove edges.

Meanwhile, adjusting the geometry of the framing columns during the Bosch-etching process provides an extra control dimension to tailor the aspect-ratio of the SiNW structure. As seen in Figure 2e–g, spiral growth of SiNHs over more than 10 layers on the column sidewalls can be controlled into conic, uniform, and inverse conic shapes,with corresponding root-to-top diameter ratios $R \equiv D_{\mathrm{col}}^{\mathrm{root}}/D_{\mathrm{col}}^{\mathrm{top}} > 1$ of 1.8, 1, and 0.5, respectively. The diameter variations of the SiNWs at different groove levels are also extracted and displayed in Figure 2h, indicating that despite the large variation of column geometry the average diameters of SiNWs remain basically constant during the spiral growth up to 12 groove layers with only a small fluctuation of <5%. This is also a strong proof that the uniformity of the a-Si coating on the standing columns, via PECVD deposition, can be good enough to guarantee a continuous and uniform spiral growth of SiNH structures.

In order to achieve free-standing SiNH units, the completely oxidized cylinders are etched off in hydrofluoric (HF) solution, as schematically diagramed in Figure 3a,b, with a protective PR layer (coated and thinned by O_2 plasma etching to ~200 nm), lying at the roots to fix the SiNH array. Interestingly, while the larger SiNHs grown on the wider cylinders with $D_{\mathrm{col}} > 1.5$ μm are easy to collapse (see Figure S2) due to the dragging force of water/air interfacial tension experienced while pulling out of solution, the thinner SiNHs are far more robust and can withstand the whole solution processing, preserving standing gestures as shown in Figure 3c and its inset. Occasionally, remnant nanocrystalline Si layer (left by the catalyst caps) is found on top of the SiNH samples, which can be cleaned off or preserved prior to the HF etching step. The released SiNHs can be easily picked and transferred to copper grids for transmission electron microscopy (TEM) characterization. As shown in Figure S3, the helical SiNW structure is found to be crystalline after checking at multiple places, and according to the electron diffraction pattern taken at a segment specified in Figure S3b the local growth orientation is along Si ⟨220⟩ direction. Note that the growth orientation of SiNW could vary at different places during a guided growth, as witnessed in our previous works on SiNW spring structures grown on planar surface.[46,48]

The cylinders can also be partially oxidized to preserve very thin central poles, standing within the hollow SiNHs, as depicted schematically in Figure 3d,e, which can help to pin

https://dx.doi.org/10.1021/acs.nanolett.0c01265
Nano Lett. 2020, 20, 5072−5080

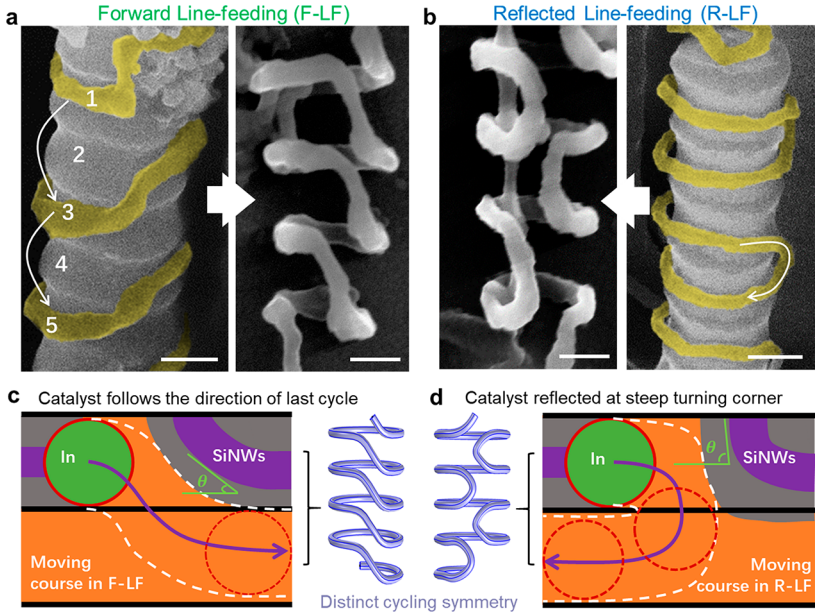

Figure 4. Line-feeding switch dynamics over groove edges. (a,b) SEM images of the SiNHs with F-LF or R-LF growth symmetry, while (c,d) sketch schematically the different switching behavior and angles over the confining groove edge lines, as well as the distinct geometries of the as-produced forward and reflected helical structures. Scale bars are all for 200 nm.

and fix the released SiNH arrays, exempting the need of the protective bottom PR layer. In addition, a thicker a-Si layer can be adopted for the growth of SiNHs, leaving a continuous remnant a-Si membrane that props the 3D helical structure and allows them to detach as a whole from the pole arrays as seen in the side view SEM images in Figure 3f,g. This provides a nice viewpoint of the slim spiral geometry against the semitransparent a-Si membrane background in the SEM imaging. Free-standing SiNHs, pinned by the Si nanopoles at precise matrix locations, are shown in Figure 3h, where the thin center poles can be preserved (the inset of Figure 3h) or broken via nanoprobe manipulation to leave hollow SiNHs (Figure 3j), which are ideal platforms for further mechanical and electric testing.

The released SiNHs reveal also more details of 3D line-feeding (LF) transition, as shown, for instance, in Figure 3c−j, which is a critical step for the droplet to linefeed into the next groove to produce continuous spiral SiNHs. Surprisingly, there are two distinct LF transition modes, that is, the forward line-feeding (F-LF) and the reflected line-feeding (R-LF) modes, which lead to chiral or achiral spiral SiNHs, respectively, as seen in Figure 4a,b for the free-standing ones or in Figure S4a,b for the SiNHs grown on thicker column sidewalls. Actually, the LF transitions are enforced at the end of each growth cycle, when the droplets run into the previous segments of SiNW (depicted schematically in Figure 4c,d). Attracted by the only available a-Si supply on the groove edges, the droplets will climb over the edges to move along the boundaries of the remnant a-Si zones. It is found that if the intersect angle between the a-Si boundary (parallel to the previous segment of turning SiNW) and the horizontal groove is small with $\theta_{FLF} \leq 45°$, the droplet will be allowed to keep a forward spiral growth in the new groove, as shown in Figure 4c. Interestingly, the F-LF transiting droplets can switch into the nearest neighbor groove (as seen in Figure 1d, Figure 3g, or Figure S5a) for the relatively wider grooves or to the next nearest neighborhood (Figure 1a) for the more compact structures. On the contrary, if the intersect angle is large $\theta_{R\text{-}LF} \geq 80°$ (see Figure 4d), the droplet will be reflected away to move in the opposite direction at each R-LF transitions. It is remarkable that both the forward or reflected LF transitions will happen at more or less the same positions, and the resulting SiNW turning segments will enforce basically the same LF transition modes for the next runs; in other words, these 3D spiral growth ordering or symmetry can be well preserved during the helical growth of SiNHs.

The free-standing SiNHs, with tunable 3D geometry, density, and orientations, are suitable for exploring many novel applications, for example, to serve as elastic spring supports for a building hybrid nanoscale complex, as seen in Figure 5a, where a larger PS ball is attached to the end of a standing SiNH by using a nanomanipulator in SEM, and welded by *in situ* amorphous carbon (a-C) deposition. Pulling testing of the spring-ball complex reveals that the SiNH spring can be repetitively stretched to >140%, as shown in Figure 5c,d. In addition, the current−voltage (I−V) characteristics of another standing SiNH were also tested under varied stretching strains, as shown in Figure S5a−d, by using a probe directly connected to the tip of the SiNH (fixed by a-C layer). Despite a poor Schottky contact between the probe and the SiNH that limits the transport current to only nano-amperes, the current is found to increase by more than 120% under stretching to 240% (Figure S5d), which could arise from the piezoresistance effect of c-Si or the improved electric contact under stretching. In comparison, for the SiNH spring coated with 20 nm Au, an Ohmic contact is achieved with very stable and much higher transport current of about micro-amperes even under stretching to 150% strain, see Figure S5e,f.

The standing SiNHs are ideal resonators that can be electrically driven and excited to distinct resonant modes at different frequencies. For instance, a SiNH unit with 7.5 period of spiral cycles is chosen and approached by a tungsten probe in an SEM chamber with the experimental setup and SEM image shown in Figure 5d,e, respectively. The probe is kept ∼1

https://dx.doi.org/10.1021/acs.nanolett.0c01265
Nano Lett. 2020, 20, 5072−5080

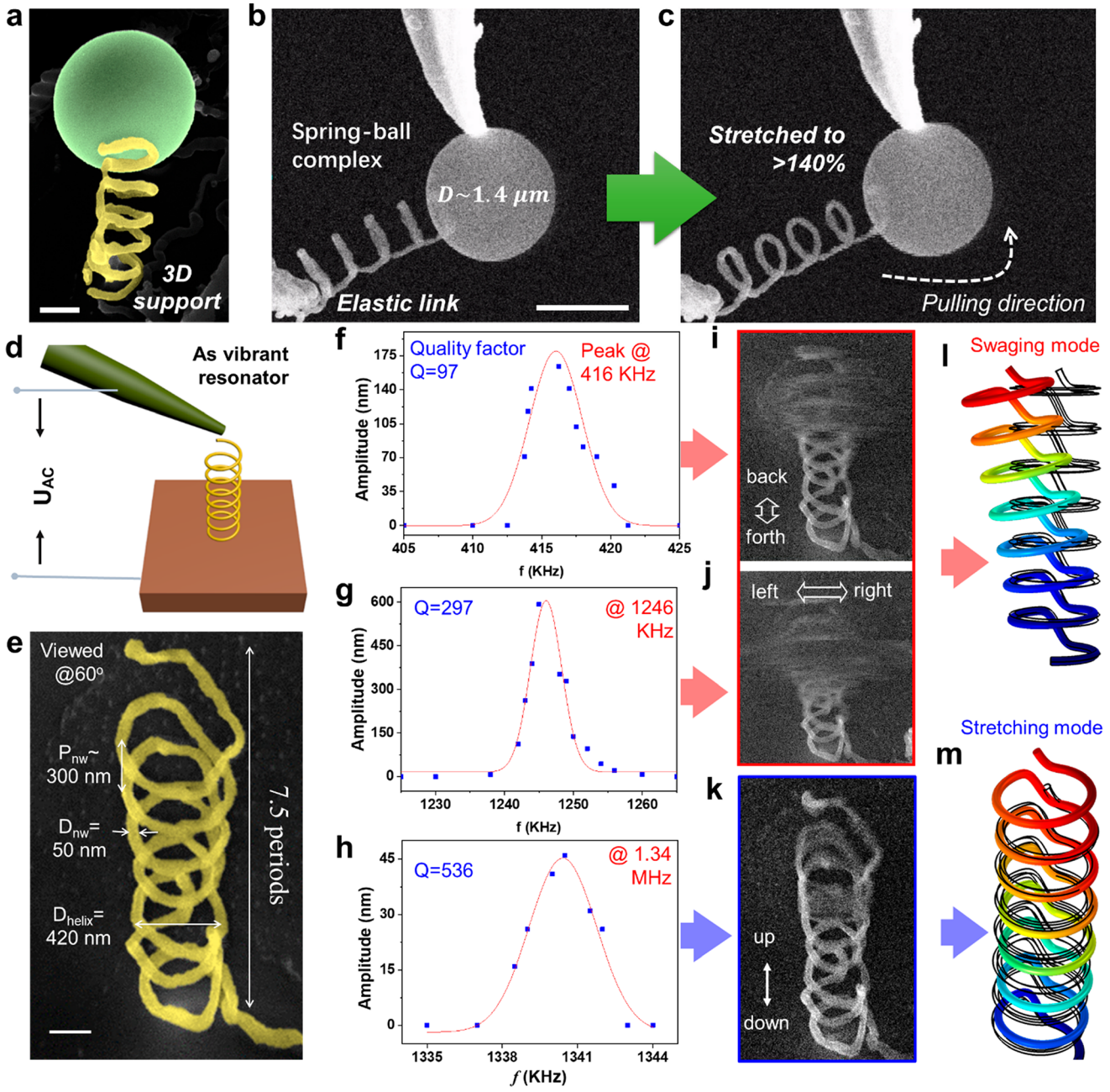

Figure 5. (a–c) The SEM images of the SiNHs serving as 3D support for hybrid spring-ball complex and super elastic link before/under large stretching strain. Scale bar in (a) stands for 400 nm and in (b,c) for 1 μm. (d) The experimental setup standing SiNH resonator testing with an SEM image shown in (e). (f–h) The vibration amplitude peaks for three different resonant modes with corresponding vibration SEM images presented in (i–k), respectively. According to finite element modeling and simulation analysis, the first two resonant frequencies are assigned to the swaging resonant modes (l) while the last one is assigned to an up–down stretching mode (*m*). The color rendering in the SiNHs that varied from red to blue signifies the magnitude of displacement (from large to zero) in the resonant modes. Scale bar in (e) is 200 nm.

apart from the tip of SiNH, applying an alternating voltage of 5 V amplitude with frequency ramping from 1 kHz to 10 MHz. Alhough the scanning rate of SEM observation is too low to resolve the vibrational details, the vibration causes blurring in the imaging that can be used to extract the amplitude and gesture of the resonating SiNHs. For this SiNH resonator, three resonant peaks located at 0.42, 1.246 and 1.34 MHz were identified in the plots of vibration amplitude against the frequency scan in Figure 5f–h, respectively. According to the corresponding SEM images presented in Figure 5i–k, the lowest two resonant modes can be assigned to the swaging of the standing SiNH in back–forth and left–right manners, while the last one is of a typical up–down stretching mode vibrating along the *z*-axis direction. Finite element simulation was also carried out by using COMSOL analysis toolkit, where the SiNH is modeled by a standing helical spring composed of uniform poly-Si materials with an isotropic Young modulus of 160 GPa and corresponding geometry/material parameters specified in Figure S6. The vibrational deformations of the lowest swaging and stretching modes are calculated and plotted Figure 5l,m, respectively, which resemble indeed the vibrational features observed under the *in situ* excitations.

https://dx.doi.org/10.1021/acs.nanolett.0c01265
Nano Lett. 2020, 20, 5072–5080

However, due to the inhomogeneous bottom fixation, the geometry fluctuation of the SiNH, and the possible lower Young's modulus in the actual SiNH arising from the existence of structural defects and a softer oxide layer on the sidewalls, the calculated frequencies are found to be 4−6 times higher than the experimental observations.

In summary, a novel 3D spiral growth of Si nanohelices (SiNHs) has been demonstrated, for the very first time, directly upon corrugated sidewalls of bamboolike cylinders. The sidewall grooves provide precise lateral guidance for the formation of compact and slim SiNHs, where a continuous helical growth is guaranteed by unique line-feeding dynamics that happens at the end of each growth loop cycle. These SiNH arrays can be batch-manufactured with programmable diameter, layer pitch, and geometry aspect-ratio and can be reliably released into self-standing units to serve as elastic links, supports, and vibrant resonators. These results highlight the unique potential of IPSLS growth mechanism in constructing more sophisticated and advanced 3D NEMS and optoelectronic applications.

EXPERIMENTAL SECTION

Bosch Etching and Oxidation of Bamboolike Pillars. Si (100) wafer substrates (2 × 2 cm) were cleaned by using acetone, ethanol, and deionized water ultrasonically for 5 min, prior to covering a monolayer PS sphere monolayer. The diameter of the PS spheres and thus that of the etched pillars, were reduced by O_2 plasma etching in inductive coupled plasma (ICP, Oxford 180) system with O_2 flow rate, chamber pressure, and ICP power of 20 standard cubic centimeter (SCCM), 20 mTorr, and 500 W, respectively. Then, Bosch etching process was used to etch into the underlying Si wafer to produce bamboolike pillars with typically SF_6 etching cycle duration of 11 s with flow rate, pressure, and power of 100 SCCM, 22 mTorr, and 700 W, respectively. Then, a C_4F_8 passivation cycle was carried out with duration of 8 s with flow rate, pressure, and power of 100 SCCM, 30 mTorr, and 600 W, respectively. The etching and the passivation cycles were then repeated for N_{layer} = 6−12 times to produce corrugated pillars with a corresponding number of groove layers. The gas flow rates and the processing durations for the etching and passivation are used as the primary control parameters to adjust the profile of the sidewall grooves. At the end, the Si pillars were partially or completely oxidized in (1) a dry O_2 ambient to preserve a thin Si pillar cores or (2) a wet O_2/H_2O ambient, respectively, with 100 SCCM N_2 carrier gas at 1000 °C for 0.5−3 h.

Selective In Catalyst Deposition and Droplet Formation. The samples were then spin-coated with photoresist (AZ5214) at 500/4000 rpm for 5/40 s and baked at 100 °C for 1 min, then the photoresist layer was reduced by O_2 plasma in reactive ion etching (RIE, Samco 10NR) system with 10 Pa, 50 W for 3−5 min to expose only the top segment (30−60 nm) of the pillars. Then, a thin layer of In catalyst of nominally 30−40 nm thick was evaporated by using thermal evaporation or EBE sputtering. After that, the photoresist was removed in acetone ultrasonically and the samples were dried by pure N_2 flow and loaded into the chamber of the PECVD system, where a H_2 plasma treatment at 200 to 250 °C with gas flow rate, chamber pressure, and RF power of 14 SCCM, 140 Pa and 10 W was applied for 5−8 min. The H_2 plasma can help to remove the native oxide layer on the surface of the In particles, allowing them to migrate and agglomerate into discrete droplets with tunable diameter by controlling the plasma condition and the initial In layer thickness.

a-Si Coating and SiNW Growth. The a-Si layer was deposited by using 4 SCCM pure silane (SiH_4) plasma at a lower temperature of 150 °C with 20 Pa pressure and 2 W RF power for 8−10 min. Then, the substrate temperature was raised to 300 °C while kept in vacuum for 1 h. During this course, the catalyst droplet became molten again and started to absorb a-Si layer as a precursor to produce SiNWs, via an IPSLS growth mechanism, and move from the top of the pillars into the sidewall grooves. The catalyst droplets with proper size matching the groove profile will first move along the parallel groove loops and run into itself at the end of each cycle which then forced the droplets to switch into the next vacant groove below to produce a continuous SiNW. At the end of the SiNW growth, the remnant a-Si layer can be preserved or selectively removed by using H_2 plasma etching at 150 °C with typical gas flow rate, chamber pressure, and RF power of 14 SCCM, 140 Pa, and 20 W, respectively, for 12 min.

SiNHs Releasing from the Columns. To release the sidewall-grown continuous SiNWs into self-standing nanohelices, the partially or completely oxidized Si or silica columns were etched in a 4% HF solution for 2−10 s and then baked at 100 °C on heating stage in air. Prior to the etching, a thin layer of photoresist of 40−200 nm can be applied at the roots of the pillar, which can help to fix the SiNHs. Specifically, the photoresist layer was first coated upon the sample surface and baked at 100 °C for 1 min, followed by an O_2 plasma at 10 Pa, 50 W for 10−15 min reducing the photoresist layer to the desired thickness. For the SiNHs with center narrow pillars left by partial oxidation of the columns, the bottom photoresist fixation layer is not necessary, as the SiNHs are anchored by the central pillars at the original positions, even going through the solution etching process.

Spring-ball Complex Fabrication. First, standing SiNH array of specific diameters were fabricated upon Si wafer substrates, fixed by photoresist layer at the bottom, and released as self-standing units by HF etching. In order to place the PS sphere on the top of the SiNHs, freestanding SiNHs fabricated on n+-Si wafer substrate were mounted upon 60° tilted stage in the SEM system. The relatively large PS spheres (diameter >1 micro) were placed on the nearby surface on the wafer substrate beforehand. After marking the targeted SiNH, the PS sphere was picked up by a nanomanipulator integrated in the SEM chamber and transferred to touch the end of the freestanding SiNH. Amorphous carbon film was deposited around the touching point by focusing the electron beam (that breaks the leaked carbonate or organic gas molecules) for 1−5 min, which can help to solder the PS particle to the end of the SiNH spring with a reasonable adhesion strength but not a good electric contact.

Stretching IV and Resonant Vibration Characterizations. The stretching manipulation and resonant vibration measurements were performed by using a pair of tungsten manipulators. For the stretching $I-V$ characterization of a targeted SiNH spring, one of the tungsten probes was welded with the top of the SiNH by depositing a-C layer, while the other one was contacted with the nearby wafer substrate (n+-Si) surface. The electronic transport characteristic of the stretched SiNH spring was measured by using Keithley 2636B Source-Meter during the stretching. For the resonant vibration characterization, a standing SiNH spring was chosen and approached by a probe overhead (tilting 30° off the axis). The

https://dx.doi.org/10.1021/acs.nanolett.0c01265
Nano Lett. 2020, 20, 5072−5080

alternating voltage signal was provided by a frequency generator (Keithley 3390), and the vibration amplitude was monitored and recorded directly by SEM observation.

■ ASSOCIATED CONTENT

Supporting Information

The Supporting Information is available free of charge at https://pubs.acs.org/doi/10.1021/acs.nanolett.0c01265.

Figure S1: SEM images of PS template and corrugated cylinders. Figure S2: Large Si nanohelical (SiNH) structures. Figure S3: Transmission electron microscopy (TEM) characterizations. Figure S4: Line-feeding growth transition on column sidewall. Figure S5: Stretching and current−voltage (I−V) characteristics of SiNHs. Figure S6: Simulation configuration and parameters (PDF)

■ AUTHOR INFORMATION

Corresponding Author

Linwei Yu − *National Laboratory of Solid State Microstructures/School of Electronics Science and Engineering/Collaborative Innovation Center of Advanced Microstructures, Nanjing University, Nanjing 210093, P.R. China;* orcid.org/0000-0002-0801-5210; Email: yulinwei@nju.edu.cn

Authors

Haiguang Ma − *National Laboratory of Solid State Microstructures/School of Electronics Science and Engineering/Collaborative Innovation Center of Advanced Microstructures, Nanjing University, Nanjing 210093, P.R. China*

Rongrong Yuan − *National Laboratory of Solid State Microstructures/School of Electronics Science and Engineering/Collaborative Innovation Center of Advanced Microstructures, Nanjing University, Nanjing 210093, P.R. China*

Junzhuan Wang − *National Laboratory of Solid State Microstructures/School of Electronics Science and Engineering/Collaborative Innovation Center of Advanced Microstructures, Nanjing University, Nanjing 210093, P.R. China*

Yi Shi − *National Laboratory of Solid State Microstructures/School of Electronics Science and Engineering/Collaborative Innovation Center of Advanced Microstructures, Nanjing University, Nanjing 210093, P.R. China*

Jun Xu − *National Laboratory of Solid State Microstructures/School of Electronics Science and Engineering/Collaborative Innovation Center of Advanced Microstructures, Nanjing University, Nanjing 210093, P.R. China;* orcid.org/0000-0002-0469-9766

Kunji Chen − *National Laboratory of Solid State Microstructures/School of Electronics Science and Engineering/Collaborative Innovation Center of Advanced Microstructures, Nanjing University, Nanjing 210093, P.R. China*

Complete contact information is available at: https://pubs.acs.org/10.1021/acs.nanolett.0c01265

Notes

The authors declare no competing financial interest.

■ ACKNOWLEDGMENTS

The authors thank Prof. Yu Deng at Nanjing University for his help in HR-TEM analysis and acknowledge the fruitful discussion with and the helpful suggestions from Prof. Pere Roca i Cabarrocas in Ecole Polytechnique. This work receives financial support from the National Natural Science Foundation of China under Nos. 61674075, 11874198 and 61974064 and National Key R&D Program of China (2018YFB2200101 and 2018YFA0209104).

■ REFERENCES

(1) Topol, A. W.; La Tulipe, D. C.; Shi, L.; Frank, D. J.; Bernstein, K.; Steen, S. E.; Kumar, A.; Singco, G. U.; Young, A. M.; Guarini, K. W.; Ieong, M. Three-dimensional integrated circuits. *IBM J. Res. Dev.* **2006**, *50* (45), 491−506.

(2) Nam, S.; Jiang, X.; Xiong, Q.; Ham, D.; Lieber, C. M. Vertically integrated, three-dimensional nanowire complementary metal-oxide-semiconductor circuits. *Proc. Natl. Acad. Sci. U. S. A.* **2009**, *106* (50), 21035.

(3) Oh, J. Y.; Park, J.-T.; Jang, H.-J.; Cho, W.-J.; Islam, M. S. 3D-Transistor Array Based on Horizontally Suspended Silicon Nanobridges Grown via a Bottom-Up Technique. *Adv. Mater.* **2014**, *26* (12), 1929−1934.

(4) De Marchi, M.; Sacchetto, D.; Zhang, J.; Frache, S.; Gaillardon, P.-E.; Leblebici, Y.; De Micheli, G. Top-Down Fabrication of Gate-All-Around Vertically Stacked Silicon Nanowire FETs With Controllable Polarity. *IEEE Trans. Nanotechnol.* **2014**, *13* (6), 1029−1038.

(5) Schmidt, V.; Riel, H.; Senz, S.; Karg, S.; Riess, W.; Gosele, U. Realization of a Silicon Nanowire Vertical Surround-Gate Field-Effect Transistor. *Small* **2006**, *2* (1), 85−88.

(6) Wu, X.; Ma, H.; Yin, H.; Pan, D.; Wang, J.; Yu, L.; Xu, J.; Shi, Y.; Chen, K. 3D Sidewall Integration of Ultrahigh-Density Silicon Nanowires for Stacked Channel Electronics. *Advanced Electronic Materials* **2019**, *5* (0), 1800627.

(7) Hu, R.; Ma, H.; Yin, H.; Xu, J.; Chen, K.; Yu, L. Facile 3D integration of Si nanowires on Bosch-etched sidewalls for stacked channel transistors. *Nanoscale* **2020**, *12* (4), 2787−2792.

(8) de Lépinay, L. M.; Pigeau, B.; Besga, B.; Vincent, P.; Poncharal, P.; Arcizet, O. A universal and ultrasensitive vectorial nanomechanical sensor for imaging 2D force fields. *Nat. Nanotechnol.* **2017**, *12* (2), 156.

(9) Karabalin, R.; Feng, X.; Roukes, M. Parametric nanomechanical amplification at very high frequency. *Nano Lett.* **2009**, *9* (9), 3116−3123.

(10) Abhilash, T.; Mathew, J. P.; Sengupta, S.; Gokhale, M. R.; Bhattacharya, A.; Deshmukh, M. M. Wide bandwidth nanowire electromechanics on insulating substrates at room temperature. *Nano Lett.* **2012**, *12* (12), 6432−6435.

(11) Qing, Q.; Jiang, Z.; Xu, L.; Gao, R.; Mai, L.; Lieber, C. M. Free-standing kinked nanowire transistor probes for targeted intracellular recording in three dimensions. *Nat. Nanotechnol.* **2014**, *9* (2), 142−147.

(12) Jiang, Z.; Qing, Q.; Xie, P.; Gao, R.; Lieber, C. M. Kinked p−n Junction Nanowire Probes for High Spatial Resolution Sensing and Intracellular Recording. *Nano Lett.* **2012**, *12* (3), 1711−1716.

(13) Cao, C.; Du, H.; Xu, Y.; Zhu, H.; Zhang, T.; Yang, R. Superelastic and Spring Properties of Si3N4Microcoils. *Adv. Mater.* **2008**, *20* (9), 1738−1743.

(14) Gansel, J. K.; Thiel, M.; Rill, M. S.; Decker, M.; Bade, K.; Saile, V.; von Freymann, G.; Linden, S.; Wegener, M. Gold helix photonic metamaterial as broadband circular polarizer. *Science* **2009**, *325* (5947), 1513−5.

(15) Mark, A. G.; Gibbs, J. G.; Lee, T. C.; Fischer, P. Hybrid nanocolloids with programmed three-dimensional shape and material composition. *Nat. Mater.* **2013**, *12* (9), 802−7.

(16) Dobrokhotov, V.; Oakes, L.; Sowell, D.; Larin, A.; Hall, J.; Kengne, A.; Bakharev, P.; Corti, G.; Cantrell, T.; Prakash, T.; Williams, J.; McIlroy, D. N. Toward the nanospring-based artificial olfactory system for trace-detection of flammable and explosive vapors. *Sens. Actuators, B* **2012**, *168*, 138−148.

(17) Bell, D. J.; Sun, Y.; Zhang, L.; Dong, L. X.; Nelson, B. J.; Grützmacher, D. Three-dimensional nanosprings for electromechanical sensors. *Sens. Actuators, A* **2006**, *130−131*, 54−61.
(18) Singh, J.; Liu, L.; Ye, D. X.; Picu, R.; Lu, T. M.; Wang, G. C. Metal-coated Si springs: Nanoelectromechanical actuators. *Appl. Phys. Lett.* **2004**, *84*, 3657.
(19) Schwab, K. C.; Roukes, M. L. Putting mechanics into quantum mechanics. *Phys. Today* **2005**, *58* (7), 36−42.
(20) Matsui, S. Three-Dimensional Nanostructure Fabrication by Focused Ion Beam Chemical Vapor Deposition. In *Springer Handbook of Nanotechnology*; Bhushan, B., Ed.; Springer: Berlin, Heidelberg, 2010; pp 211−229.
(21) Huang, Z.; Bai, F. Wafer-scale, three-dimensional helical porous thin films deposited at a glancing angle. *Nanoscale* **2014**, *6* (16), 9401−9.
(22) Taschuk, M. T.; Hawkeye, M. M.; Brett, M. J. Glancing Angle Deposition. In *Handbook of Deposition Technologies for Films and Coatings*, third ed.; Martin, P. M., Ed.; William Andrew Publishing: Boston, 2010; pp 621−678.
(23) Lemma, E. D.; Spagnolo, B.; De Vittorio, M.; Pisanello, F. Studying Cell Mechanobiology in 3D: The Two-Photon Lithography Approach. *Trends Biotechnol.* **2019**, *37* (4), 358−372.
(24) Sun, H.-B.; Kawata, S. Two-Photon Photopolymerization and 3D Lithographic Microfabrication. In *NMR • 3D Analysis • Photopolymerization*; Fatkullin, N.; Ikehara, T., Jinnai, H., Kawata, S., Kimmich, R., Nishi, T., Nishikawa, Y., Sun, H. B., Eds.; Springer: Berlin, Heidelberg, 2004; pp 169−273.
(25) Williams, G.; Hunt, M.; Boehm, B.; May, A.; Taverne, M.; Ho, D.; Giblin, S.; Read, D.; Rarity, J.; Allenspach, R.; Ladak, S. Two-photon lithography for 3D magnetic nanostructure fabrication. *Nano Res.* **2018**, *11* (2), 845−854.
(26) Xu, S.; Yan, Z.; Jang, K.-I.; Huang, W.; Fu, H.; Kim, J.; Wei, Z.; Flavin, M.; McCracken, J.; Wang, R.; Badea, A.; Liu, Y.; Xiao, D.; Zhou, G.; Lee, J.; Chung, H. U.; Cheng, H.; Ren, W.; Banks, A.; Li, X.; Paik, U.; Nuzzo, R. G.; Huang, Y.; Zhang, Y.; Rogers, J. A. Assembly of micro/nanomaterials into complex, three-dimensional architectures by compressive buckling. *Science* **2015**, *347* (6218), 154.
(27) Fu, H.; Nan, K.; Bai, W.; Huang, W.; Bai, K.; Lu, L.; Zhou, C.; Liu, Y.; Liu, F.; Wang, J.; Han, M.; Yan, Z.; Luan, H.; Zhang, Y.; Zhang, Y.; Zhao, J.; Cheng, X.; Li, M.; Lee, J. W.; Liu, Y.; Fang, D.; Li, X.; Huang, Y.; Zhang, Y.; Rogers, J. A. Morphable 3D mesostructures and microelectronic devices by multistable buckling mechanics. *Nat. Mater.* **2018**, *17* (3), 268−276.
(28) Yan, Z.; Zhang, F.; Wang, J.; Liu, F.; Guo, X.; Nan, K.; Lin, Q.; Gao, M.; Xiao, D.; Shi, Y.; Qiu, Y.; Luan, H.; Kim, J. H.; Wang, Y.; Luo, H.; Han, M.; Huang, Y.; Zhang, Y.; Rogers, J. A. Controlled mechanical buckling for origami-inspired construction of 3D microstructures in advanced materials. *Adv. Funct. Mater.* **2016**, *26* (16), 2629−2639.
(29) Gao, P. X.; Ding, Y.; Mai, W.; Hughes, W. L.; Lao, C.; Wang, Z. L. Conversion of Zinc Oxide Nanobelts into Superlattice-Structured Nanohelices. *Science* **2005**, *309* (5741), 1700.
(30) Zhang, D.; Alkhateeb, A.; Han, H.; Mahmood, H.; McIlroy, D. N.; Norton, M. G. Silicon Carbide Nanosprings. *Nano Lett.* **2003**, *3* (7), 983−987.
(31) Shen, G. Z.; Bando, Y.; Zhi, C. Y.; Yuan, X. L.; Sekiguchi, T.; Golberg, D. Single-crystalline cubic structured InP nanosprings. *Appl. Phys. Lett.* **2006**, *88* (24), 243106.
(32) Moore, D.; Ding, Y.; Wang, Z. L. Hierarchical structured nanohelices of ZnS. *Angew. Chem., Int. Ed.* **2006**, *45* (31), 5150−4.
(33) Shen, G.; Liang, B.; Wang, X.; Chen, P.-C.; Zhou, C. Indium Oxide Nanospirals Made of Kinked Nanowires. *ACS Nano* **2011**, *5* (3), 2155−2161.
(34) Sone, E. D.; Zubarev, E. R.; Stupp, S. I. Supramolecular templating of single and double nanohelices of cadmium sulfide. *Small* **2005**, *1* (7), 694−7.
(35) Liu, Y.; Wang, J.; Kim, S.; Sun, H.; Yang, F.; Fang, Z.; Tamura, N.; Zhang, R.; Song, X.; Wen, J.; Xu, B. Z.; Wang, M.; Lin, S.; Yu, Q.; Tom, K. B.; Deng, Y.; Turner, J.; Chan, E.; Jin, D.; Ritchie, R. O.; Minor, A. M.; Chrzan, D. C.; Scott, M. C.; Yao, J. Helical van der Waals crystals with discretized Eshelby twist. *Nature* **2019**, *570* (7761), 358−362.
(36) Shadmi, N.; Kremen, A.; Frenkel, Y.; Lapin, Z. J.; Machado, L. D.; Legoas, S. B.; Bitton, O.; Rechav, K.; Popovitz-Biro, R.; Galvão, D. S.; Jorio, A.; Novotny, L.; Kalisky, B.; Joselevich, E. Defect-Free Carbon Nanotube Coils. *Nano Lett.* **2016**, *16* (4), 2152−2158.
(37) Nakar, D.; Gordeev, G.; Machado, L. D.; Popovitz-Biro, R.; Rechav, K.; Oliveira, E. F.; Kusch, P.; Jorio, A.; Galvão, D. S.; Reich, S.; Joselevich, E. Few-Wall Carbon Nanotube Coils. *Nano Lett.* **2020**, *20* (2), 953−962.
(38) Rurali, R. Colloquium: Structural, electronic, and transport properties of silicon nanowires. *Rev. Mod. Phys.* **2010**, *82* (1), 427.
(39) Schmidt, V.; Wittemann, J. V.; Gösele, U. Growth, Thermodynamics, and Electrical Properties of Silicon Nanowires†. *Chem. Rev.* **2010**, *110* (1), 361−388.
(40) Wagner, R. S.; Ellis, W. C. Vapor-Liquid-Solid Mechanism of Single Crystal Growth (New Method Growth Catalysis from Impurity Whisker Epitaxial + Large Crystals Si E). *Appl. Phys. Lett.* **1964**, *4* (5), 89.
(41) Yu, L.; Alet, P.-J.; Picardi, G.; Roca i Cabarrocas, P. An In-Plane Solid-Liquid-Solid Growth Mode for Self-Avoiding Lateral Silicon Nanowires. *Phys. Rev. Lett.* **2009**, *102* (12), 125501.
(42) Yu, L.; Roca i Cabarrocas, P. Growth mechanism and dynamics of in-plane solid-liquid-solid silicon nanowires. *Phys. Rev. B: Condens. Matter Mater. Phys.* **2010**, *81* (8), 085323.
(43) Xue, Z.; Xu, M.; Zhao, Y.; Wang, J.; Jiang, X.; Yu, L.; Wang, J.; Xu, J.; Shi, Y.; Chen, K.; Roca i Cabarrocas, P. Engineering island-chain silicon nanowires via a droplet mediated Plateau-Rayleigh transformation. *Nat. Commun.* **2016**, *7*, 12836.
(44) Sun, Y.; Dong, T.; Yu, L.; Xu, J.; Chen, K. Planar Growth, Integration, and Applications of Semiconducting Nanowires. *Adv. Mater.* **2019**, *31*, 1903945.
(45) Sun, Y.; Dong, T.; Wang, J.; Xu, J.; Chen, K.; Roca i Cabarrocas, P.; Yu, L. Meandering growth of in-plane silicon nanowire springs. *Appl. Phys. Lett.* **2019**, *114* (23), 233103.
(46) Xue, Z.; Xu, M.; Li, X.; Wang, J.; Jiang, X.; Wei, X.; Yu, L.; Chen, Q.; Wang, J.; Xu, J.; Shi, Y.; Chen, K.; Roca i Cabarrocas, P. In-Plane Self-Turning and Twin Dynamics Renders Large Stretchability to Mono-Like Zigzag Silicon Nanowire Springs. *Adv. Funct. Mater.* **2016**, *26* (29), 5352−5359.
(47) Yu, L.; Roca i Cabarrocas, P. Initial nucleation and growth of in-plane solid-liquid-solid silicon nanowires catalyzed by indium. *Phys. Rev. B: Condens. Matter Mater. Phys.* **2009**, *80* (8), 085313−5.
(48) Xue, Z.; Sun, M.; Zhao, Y.; Tang, Z.; Dong, T.; Wang, J.; Wei, X.; Yu, L.; Chen, Q.; Xu, J.; Shi, Y.; Chen, K.; Roca i Cabarrocas, P. Deterministic line-shape programming of silicon nanowires for extremely stretchable springs and electronics. *Nano Lett.* **2017**, *17*, 7638.

https://dx.doi.org/10.1021/acs.nanolett.0c01265
Nano Lett. 2020, 20, 5072−5080